PROCEEDINGS, 50th Workshop on Geothermal Reservoir Engineering
Stanford University, Stanford, California, February 10-12, 2025
SGP-TR-229

Coupled Managed Pressure and Temperature Drilling in Geothermal and HPHT Wells

Xu Duan, Yifan Zhang, Pradeepkumar Ashok, Dongmei Chen, Eric van Oort

The University of Texas at Austin, Austin, TX, 78712

xuduan@utexas.edu

Keywords: geothermal wells, high-pressure high temperature (HPHT) wells, managed pressure drilling (MPD), managed temperature drilling (MTD), managed pressure and temperature drilling (MPD-MTD), reduced drift flux model (RDFM), single-input, single-output control (SISO), multi-input multi-output control (MIMO), system identification.

ABSTRACT

Drilling geothermal and high-pressure, high-temperature (HPHT) wells can present significant challenges to drilling automation and well control due to extreme formation temperatures and elevated pressures. Proactive management of both downhole pressure and temperature is crucial to maintaining wellbore integrity, ensuring the functionality of downhole tools, and preventing well loss. Despite separate advancements in managed pressure drilling (MPD) and managed temperature drilling (MTD), integrated managed pressure and temperature drilling (MPD-MTD) has not yet been addressed. This paper introduces an integrated MPD-MTD control framework based on improved reduced drift-flux model (RDFM) that incorporates temperature dynamics, interface mass transfer, and a new lumped pressure dynamics model to describe geothermal and HPHT drilling. The proposed MPD-MTD control strategy utilizes MPD choke adjustments, flow rate modulation, and mud cooling to simultaneously regulate downhole pressure and temperature.

System identification techniques are adopted to develop a reduced-order model that captures the key thermal-pressure dynamics. This reduced model simplifies the thermal-hydraulic interactions, allowing for efficient and yet accurate controller design. Based on this reduced-order model, a multi-input-multi-output (MIMO) controller was developed to simultaneously control both the bottomhole pressure and temperature. Simulations were conducted to demonstrate the utility of the developed MIMO controller. Various drilling scenarios and control actuations were evaluated, showing that the proposed integrated MPD-MTD under the MIMO control framework outperforms the decoupled MPD and MTD control strategies with respect to the stabilization time, overshot, and robustness for both downhole temperature and pressure.

1. INTRODUCTION

Geothermal energy, as one of important sustainable energy sources, remains significantly underutilized due to the challenges it faced in the well construction phase. The exploitation of high-enthalpy geothermal reservoirs, with temperatures exceeding 300°F, is essential to achieve energy production and commercial applications (Fallah et al., 2021; Khaled et al., 2023). As outlined by van Oort et al. (2021), the widespread utilization of geothermal energy is still hindered by technical, operational, and economic challenges during the drilling and completion of geothermal wells. More specifically, main difficulties facing the construction of geothermal and high-pressure high-temperature (HPHT) wells are the control of elevated downhole temperatures and pressure encountered in the extreme downhole environment. In such drilling scenarios, a simple lapse in well control can lead to kicks/losses, wellbore integrity problems, tool overheating failures, etc., which ultimately lead to substantial non-productive time (NPT). Among them, the primary limitation that prevents the drilling of deeper or more cost-effective wells is the failure of tools and sensors under extreme downhole thermal conditions, especially in high-enthalpy geothermal and high temperature oil and gas wells. Although high-temperature drilling tools, rated for up to 350°F and in select cases up to 570°F, are available, their reliability is still questionable when operated in such harsh environments (Chatterjee et al., 2015). Recently, approaches that integrate advanced pressure and temperature control while drilling have been developed to address these challenges. Such methods are effectively combined with existing thermo-hydraulic models to achieve precise well control, thereby improving the operational reliability and economic viability of geothermal wells. However, existing methods control the downhole pressure and temperature through separately using managed pressure drilling (MPD) and managed temperature drilling (MTD), but do not yet consider the interaction between downhole hydraulics and thermodynamics. A strategy that simultaneously controls both pressure and temperature through integrated MPD and MTD is needed.

In order to develop an integrated MPD-MTD control framework, an essential first step is to develop a model to describe downhole thermal-hydraulics behavior. In terms of well thermo-hydraulic model, the one-dimensional two-phase Baer and Nunziato (BN) model is widely adopted, where seven hyperbolic partial differential equations (PDE) are used to describe the two-phase mass, momentum, and energy conservation, as well as the volume advection behavior (Baer & Nunziato, 1986). When the momentum transfer between the liquid and the gas phases is simplified using an algebraic equation, the drift-flux model (DFM) is obtained (Fallah et al., 2020; Xu et al., 2019; Yang et al., 2019). Sometimes DFMs further ignore the total energy equations, which results in a simplified, 3-PDE DFM (Fjelde et al., 2003; Udegbunam et al., 2014). The 3-PDE and 4-PDE DFMs are the most widely reported models in the literature for two-phase flow modeling in well construction applications, exhibiting superior computational stability and higher fidelity.

Reduced Drift Flux Models (RDFMs) are simplified from Drift-Flux Models (DFMs) to enhance efficiency in the modeling of complex two-phase flow systems. DFMs, known for their ability to accurately capture detailed phase interactions and flow patterns, offer high precision but are computationally too demanding for real-time applications in well construction. RDFMs address this limitation by

simplifying pressure wave dynamics while retaining the essential temperature and mass transfer dynamics. Specifically, the "No Pressure Wave" (NPW) assumption in RDFMs alleviates the stringent Courant-Friedrichs-Lewy (CFL) condition, enabling numerical stability with larger time steps and reduced computational costs. This makes RDFMs a more practical and efficient choice for real-time pressure and temperature control applications.

Control of downhole pressure and temperature has also been extensively studied. Building on the advancements in two-phase flow model, especially the RDFM, recent research efforts have emphasized the integration of well control objectives to address the challenges of bottomhole pressure (BHP) or bottomhole circulating temperature (BHCT) regulation. Ma et al. (2016) proposed a choke model and a Proportional-Integral (PI) controller for BHP control. Aarsnes (2016) proposed a BHP control algorithm based on the simplified well hydraulics, which highlighted the effects of liquid-gas transport velocity differences and pressure wave velocities. The choke control algorithm was later improved by Ambrus et al. (2017) to handle both single- and two-phase flow. In addition, a Bayesian network was also adopted by these authors to detect a variety of well control events that can lead to degraded system conditions. The identified system conditions were subsequently used to update the chock response based on a process control model. Gu et al. (2019) incorporated thermodynamics into the RDFM and proposed an MPD control approach that delivered high-precision control by solving the energy equation using an explicit finite-difference method (FDM). This method provided a real-time dynamic temperature profile with minimal computational expense. Recently, Luu et al. (2024) developed the PID controller for MTD using this RDFM approach. The surface temperature and mud pump rate were adopted as control inputs.

In this paper, RDFM, system identification techniques, and control algorithms are unified into a coupled MPD-MTD framework. The advanced temperature dynamics, interface mass transfer, and improved pressure dynamics are integrated to identify the transfer function between surface temperature, pump rate, choke opening, and BHP/BHCT, forming a control-oriented reduced-order model. Surface temperature and mud pump rate, or mud pump rate and choke opening, are selected as the control input to simultaneously control the downhole temperature and pressure. These improvements enable the accurate prediction and management of bottomhole conditions in elevated temperature and pressure environments. The key contributions of this work are: (1) System identification techniques were employed to derive a simplified yet effective control model that accurately represents the coupled pressure and temperature dynamics in drilling systems; (2) A robust multi-input-multi-output (MIMO) control strategy was developed, enabling the simultaneous regulation of downhole pressure and temperature in real time, addressing the complex interactions present in geothermal and HPHT wells; (3) Extensive simulations were conducted to validate the proposed MPD-MTD control strategy.

2. THERMO-HYDRAULIC MODELING AND CONTROL FRAMEWORK

2.1 Summary of RDFM

The governing equations that define the RDFM can be categorized into three categories: pressure equations, temperature equations, and liquid and gas propagation equations. A full derivation of the RDFM can be found in Gu et al. (2022) but a brief summary is presented here for convenience.

2.1.1 Pressure Equations

Eqs. 1-3 describe the lumped pressure dynamics model used in RDFM.

$$p(x) = p_L - \int_x^L \left[f_{grav}(\xi) + f_{wf}(\xi)\right] d\xi \tag{1}$$

$$p_L = p_{L,ex} \tag{2}$$

$$\frac{dp_L}{dt} = \frac{\bar{\beta}}{V}\left(q_{l,src} + q_{g,src} + \dot{V}_{E_l,T} + \dot{V}_{E_g,S} + \dot{V}_{conv} - q_L\right) \tag{3}$$

Eq. 1 describes the pressure distribution within the well, where p_L represents the pressure at the outlet boundary, f_{grav} is the gravitational force per unit volume, and f_{wf} denotes the wall friction force per unit volume. Eq. 2 and Eq. 3 are the pressure boundary condition for open and closed system, respectively. In Eq. 2, $p_{L,ex}$ is the exogenous pressure at the outlet boundary. In Eq. 3, $\bar{\beta}$ is the effective bulk modulus, and V represents the total volume of the pipe of annulus. $q_{l,src}$ and $q_{g,src}$ refer to the flow rate of the liquid source and gas source, respectively. $\dot{V}_{E_l,T}$ is the volume source term related to liquid expansion due to temperature variation. $\dot{V}_{E_g,S}$ and $\dot{V}_{conv}$ denote the volume source term corresponding to the gas expansion and fluid convection. Finally, q_L is the volumetric flow rate at the outlet boundary.

Since the temporal variation of pressure is entirely governed by the outlet boundary pressure p_L, this approach is referred to as the "lumped pressure dynamics model". For an open system, p_L is determined exogenously using Eq. 2, while for a closed or restricted system, it is computed using Eq. 3. Once p_L is obtained, the fluid pressure profile within the well can be calculated using Eq. 1, which accounts for the effects of gravitational force and wall friction.

2.1.2 Liquid and Gas Propagation Dynamics

For calculating liquid and gas propagation dynamics, we use the mass conservation relations shown in Eqs. 4-5.

$$\frac{\partial[\alpha_l(\rho_l - \rho_g^*)]}{\partial t} + \frac{\partial[\alpha_l(\rho_l - \rho_g^*)v_l]}{\partial x} = \Gamma_{m,l} \tag{4}$$

$$\frac{\partial[\alpha_g\rho_g-\alpha_l\rho_g^\star]}{\partial t}+\frac{\partial[\alpha_g\rho_g v_g-\alpha_l\rho_g^\star v_l]}{\partial x}=\Gamma_{m,g} \tag{5}$$

where α_l and α_g are the volume fractions of liquid and gas, respectively. ρ_l and ρ_g are the density of gas and liquid, respectively. $\rho_g^\star$ represents the equivalent density of the dissolved gas. $\Gamma_{m,l}$ and $\Gamma_{m,g}$ are the rate of mass generation from sources per unit volume.

Eq. 4 and Eq. 5 are solved separately to obtain the liquid/gas volume fractions and equivalent density of the dissolved gas, with the velocities v_g and v_l being calculated explicitly using the Eqs. 6-7.

$$v_g(x)=e^{-I_v(x)}\left\{\int_0^x C_0 e^{I_v(\zeta)}\left[-\frac{\alpha_g}{\rho_g}\left(\frac{\partial\rho_g}{\partial p}\frac{\partial p}{\partial t}+\frac{\partial\rho_g}{\partial T}\frac{\partial T}{\partial t}\right)+\frac{\Gamma_{m,g}-\Gamma_d}{\rho_g}+\frac{\Gamma_{m,l}-\Gamma_d}{\rho_l}+\frac{1}{C_0}\frac{\partial v_d}{\partial x}\right]d\zeta+v_{g,o}\right\} \tag{6}$$

$$v_l(x)=\frac{(1-C_0\alpha_g)v_g-v_d}{C_0\alpha_l} \tag{7}$$

where v_d is the drift velocity and C_0 is the distribution parameter.

2.1.3 Thermodynamics

The thermal processes in typical drilling operations primarily involve conduction and convection mechanisms. Conduction occurs radially through the pipes, cement, and formation. Axial conduction within the formation is typically neglected due to its minimal impact. Convection processes include axial and radial convection within the pipe and annulus mud flow, as well as natural convection in the surrounding seawater for offshore applications. The dynamics of these thermal processes are governed by the energy conservation equation, as presented in Eq. 8.

$$\frac{\partial(\alpha_l\rho_l e_l+\alpha_g\rho_g e_g)}{\partial t}+\frac{\partial(\alpha_l\rho_l v_l h_l+\alpha_g\rho_g v_g h_g)}{\partial x}=\dot{Q}_{ht}+\Gamma_{h,all}+\dot{Q}_{bit} \tag{8}$$

In this equation, e is the energy per unit mass, and h denotes the enthalpy per unit mass. The relationships are further defined by Eqs. 9-10.

$$e=c_vT+gs \tag{9}$$

$$h=e+\frac{p}{\rho} \tag{10}$$

Here c_v is the specific heat capacity at constant volume, T is the temperature, g is the gravitational acceleration, and s is the vertical position.

On the RHS of Eq. 8, three source terms are defined: $\dot{Q}_{ht}$, the rate of heat transfer through the walls per unit volume, considers all the radial conduction and convection; $\Gamma_{h,all}$, the rate of total enthalpy generation from all sources per unit volume, considers the influence of mass transfer between the annulus mud flow and the surrounding formation and reservoir; $\dot{Q}_{bit}$, the rate of heat flux from the bit per unit volume. $\Gamma_{h,all}$ and $\dot{Q}_{bit}$ can usually be determined exogenously from the given information about the mass sources, the bit, and the drilling operation conditions. $\dot{Q}_{ht}$ on the other hand, requires a heat transfer network to calculate the transient heat transfer rate between the mud, the drillstring, the casing, the cement, and the formation. A heat transfer network proposed by Fallah et al. (2020) is applied in this research. The details are shown in Figure 1: Schematic of heat transfer network. 1. Heat transfer between drillstring fluid and the annulus fluid. 2. Heat transfer between the annulus fluid and the formation in the open hole. 3. Heat transfer between the annulus fluid and the formation in the cased hole. Adapted from Fallah et al. (2020)

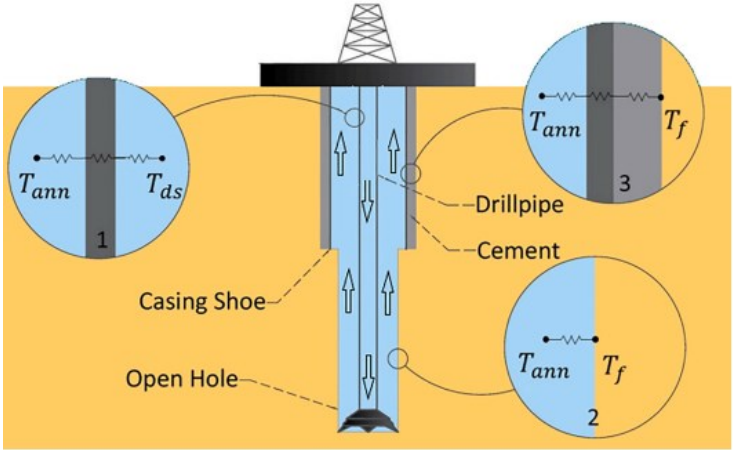

Figure 1: Schematic of heat transfer network. 1. Heat transfer between drillstring fluid and the annulus fluid. 2. Heat transfer between the annulus fluid and the formation in the open hole. 3. Heat transfer between the annulus fluid and the formation in the cased hole. Adapted from Fallah et al. (2020).

For the flow in a drillstring, there is only heat flux from its outer surface and $\dot{Q}_{ht}$ can be calculated as:

$$\dot{Q}_{ht} = \dot{Q}_{ht,outer} = \frac{T_{m,out} - T_{m,ds}}{R_{outer}} \tag{11}$$

For the flow in the annulus, there are heat fluxes from both its inner and outer surfaces, and $\dot{Q}_{ht}$ can be calculated as:

$$\dot{Q}_{ht} = \dot{Q}_{ht,inner} + \dot{Q}_{ht,outer} = \frac{T_{m,in} - T_{m,ann}}{R_{inner}} + \frac{T_{m,out} - T_{m,ann}}{R_{outer}} \tag{12}$$

where $\dot{Q}_{ht,outer}$ is the rate of heat transfer at the outer surface of the drillstring/annulus per unit volume; $\dot{Q}_{ht,inner}$ denotes the rate of heat transfer at the inner surface of the annulus per unit volume. $T_{m,out}$ is the temperature of the medium outside the annulus. $T_{m,ds}$ refers to the temperature of the drillstring medium. R_{outer} is the thermal resistance in the outer surface of the drillstring/annulus. Similarly, $T_{m,in}$ represents the temperature of the medium inside the annulus. $T_{m,ann}$ corresponds the temperature of the annulus medium, and R_{inner} is the thermal resistance of the inner surface of the annulus.

The inner and outer thermal resistances (R_{inner} and R_{outer}) are calculated by adding the proper conduction and convection resistances on the outer and inner sides. The conduction resistance is calculated using the typical formula for a hollow cylinder. With the non-Newtonian facts being considered, the convection resistance is calculated through the Nusselt number with various formulas, depending on whether it is laminar or turbulent flow, and whether the flow occurs in the pipe or the annulus. Moreover, the variation of the near-well formation temperature is also considered by including a dynamic meshing strategy in formation, which helps describe the cooling effect of the mud on the formation, as shown in Figure 2. Discretization of rock formation for heat transfer calculation for a cased section of the wellbore. Adapted from Fallah et al. (2021).

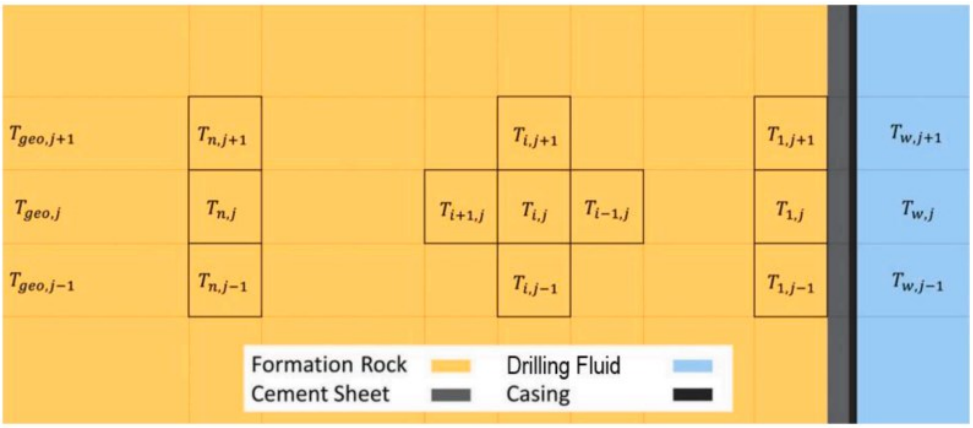

Figure 2. Discretization of rock formation for heat transfer calculation for a cased section of the wellbore. Adapted from Fallah et al. (2021).

2.1.4 Numerical Method

The aforementioned equations are supplemented by closure relations, which include the equations of state for liquid and gas, as well as the relationship between volume fractions, as defined in Eqs. 13-15.

$$\rho_l = f(p, T) \tag{13}$$

$$\rho_g = f(p, T) \tag{14}$$

$$\rho^*_{g,sat} = f(p, T) \tag{15}$$

$$\alpha_l + \alpha_g = 1 \tag{16}$$

In this paper, the RDFM uses a first-order upwind scheme in space and explicit Euler method in time. When solving the differential equations, the explicit Euler method is applied, where any differential equation with the format of Eq. 17 can be discretized as Eq. 18.

$$\frac{d\emptyset}{dt} = f(t, \emptyset) \tag{17}$$

$$\emptyset_{n+1} = \emptyset_n + f(t_n, \emptyset_n) \tag{18}$$

2.2 Control Framework

2.2.1 System Identification

System identification is beneficial for understanding a system's dynamic behavior and subsequently informing the design of its controller. For SISO systems, let the model be given by

$$Y(s) = \frac{B(s)}{A(s)}U(s) \tag{19}$$

Or in the time domain

$$y^{(n)}(t) + a_1 y^{(n-1)}(t) + \ldots + a_n y(t) = b_1 u^{(m-1)}(t) + b_2 u^{(m-2)}(t) + \ldots + b_m u(t) \tag{20}$$

where $y(t)$ is the response variable—such as the BHP or BHCT in this context. And $u(t)$ is the control variable, which may be mud pump rate Q, mud temperature at inlet T_{in}, or choke opening. Here, $y^{(k)}(t)$ denotes the k:th derivative of $y(t)$ with respect to time, and $u^{(k)}(t)$ denotes the k:th derivative of $u(t)$ with respect to time. The model coefficients can be calculated via a least-squares approach, given by

$$\theta^{LS} = \left[\sum_{i=1}^{N} \phi(t_k)\phi^T(t_k)\right]^{-1} \sum_{i=1}^{N} \phi(t_k) y^n(t_k) \tag{21}$$

$$\theta = [a_1 \quad \cdots \quad a_n \quad b_1 \quad \cdots \quad b_m]^T \tag{22}$$

$$\phi^T(t_k) = \left[-y^{(n-1)}(t_k) \quad \cdots \quad -y(t_k) \quad u^{(m)}(t_k) \quad \cdots \quad u(t_k)\right] \tag{23}$$

Additional details regarding this approach and its implementation are provided in Ljung (2009) and Garnier et al. (2003).

Using this technique, transfer functions relating the control variables to the response variables are identified. Figure 3. System identification results for mud pump rate. The mud pump rate (left) remains at 400 gpm, then increases to 600 gpm at 500 minutes. The middle panel shows BHP, and the right panel shows BHCT, with observed data compared against identification results. compare the original system with the identified system where the control variables are mud pump rate, mud temperature at inlet and choke opening, respectively. Further details about the choke model can be found in Ma et al. (2016) and Ambrus et al. (2017). Once the system reaches steady state, the control variables are changed to examine how incremental changes in these variables affect the response variables. The identified systems agree very well with the original systems.

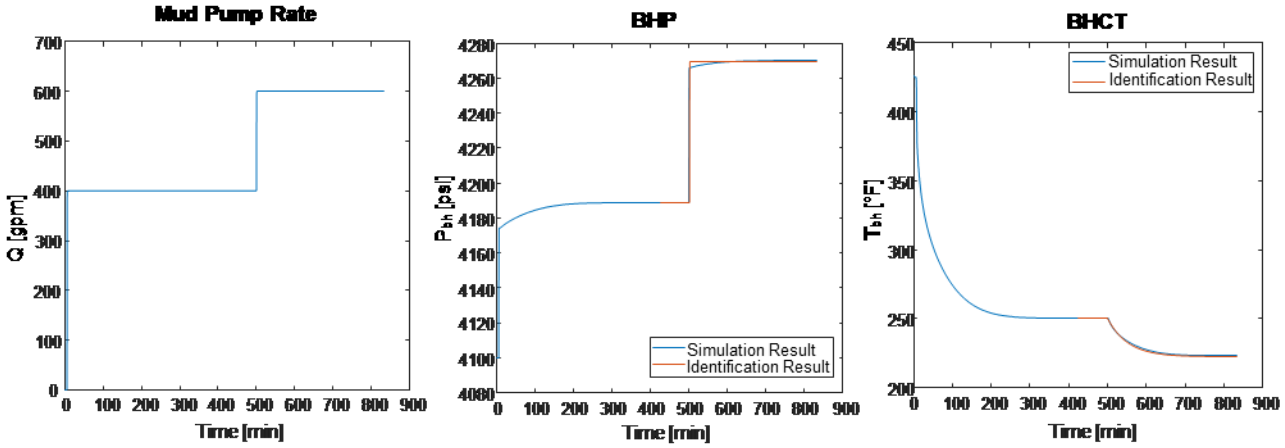

Figure 3. System identification results for mud pump rate. The mud pump rate (left) remains at 400 gpm, then increases to 600 gpm at 500 minutes. The middle panel shows BHP, and the right panel shows BHCT, with observed data compared against identification results.

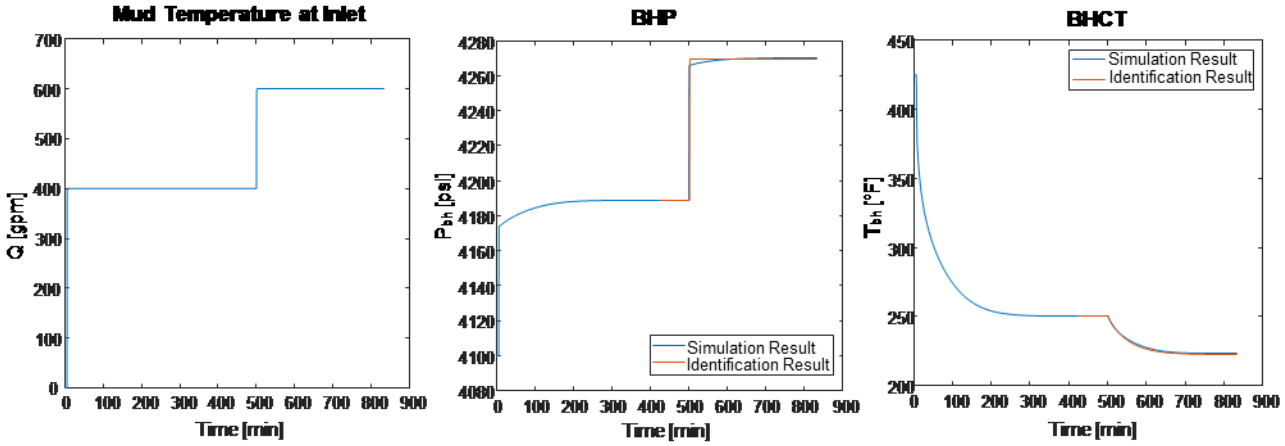

Figure 4. System identification results for mud temperature at inlet. The mud temperature at inlet (left) remains at 77 °F, then increases to 120 °F at 500 minutes. The middle panel shows BHP, and the right panel shows BHCT, with observed data compared against identification results.

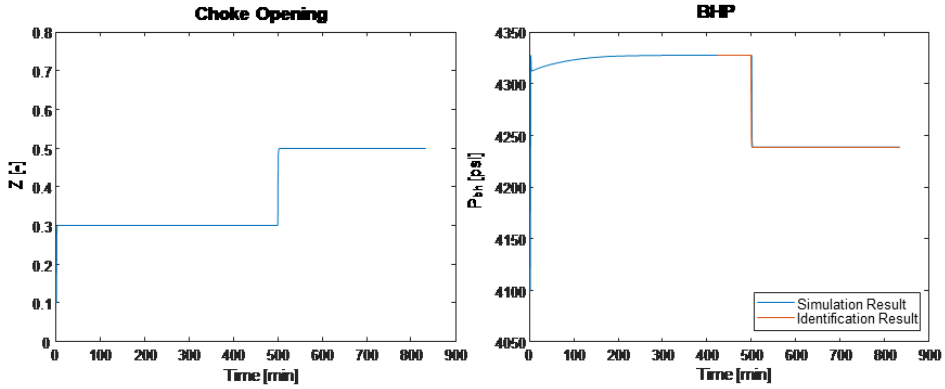

Figure 5. System identification results for choke opening. The choke opening (left) remains at 0.3, then increases to 0.5 at 500 minutes. the right panel shows BHP, with observed data compared against identification results.

2.2.2 MIMO Control Algorithm

PI controllers are utilized in the system. Specifically, PI controllers H_{ij} are designed for each identified transfer function G_{ij}. When mud pump rate and mud temperature at inlet are employed as control variables, the MIMO control diagram of is presented as in Figure 6. Control diagram of the MIMO controller. Control variables are mud pump rate and mud temperature at inlet.

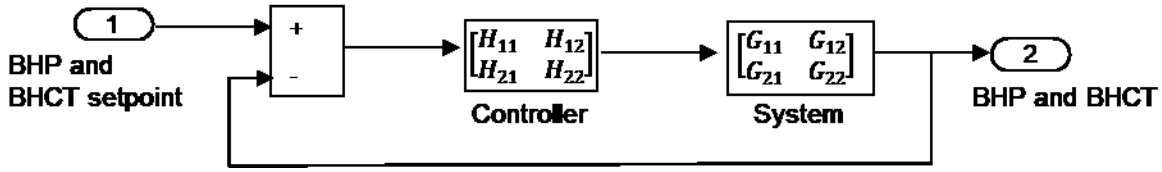

Figure 6. Control diagram of the MIMO controller. Control variables are mud pump rate and mud temperature at inlet.

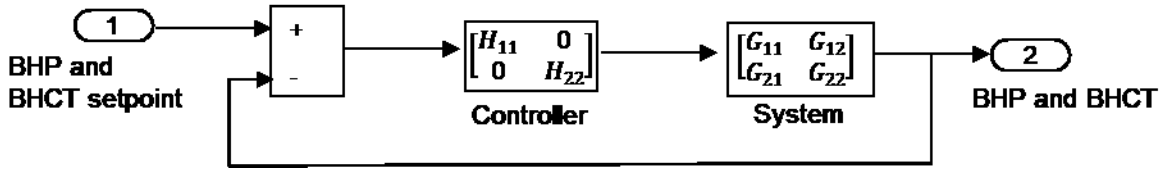

Figure 7. Control diagram of the SISO controllers. Control variables are mud pump rate and mud temperature at inlet.

The calculation of control variables is shown in Eq. 25.

$$\begin{bmatrix} P_{bh,err} \\ T_{bh,err} \end{bmatrix} = \begin{bmatrix} P_{bh,setpoint} \\ T_{bh,setpoint} \end{bmatrix} - \begin{bmatrix} P_{bh} \\ T_{bh} \end{bmatrix} \quad (24)$$

$$\begin{bmatrix} T_{in} \\ Q \end{bmatrix} = \begin{bmatrix} H_{11} & H_{12} \\ H_{21} & H_{22} \end{bmatrix} \begin{bmatrix} P_{bh,err} \\ T_{bh,err} \end{bmatrix} \quad (25)$$

To highlight the effectiveness of the coupled controller, it is compared with two SISO controllers, where the off-diagonal entries in the controller H_{ij} are set to 0. This configuration implies that the control variable T_{in} is solely regulated by BHCT, while Q is exclusively controlled by BHP, as depicted in Figure 7. Control diagram of the SISO controllers. Control variables are mud pump rate and mud temperature at inlet..

In some cases, the choke is preferable for controlling BHP. Similar MIMO and SISO control algorithms are adopted when choke opening and mud pump rate are control variables.

3. CONTROL SCENARIOS AND DISCUSSION

3.1 Well Data

The open-source Utah FORGE geothermal well dataset is used to test the MIMO controller for geothermal temperature simulation and control (Utah Forge Data, 2022). Table 8: Drilling fluid properties for Utah FORGE 16A78-32 well. and Table 9: Formation geothermal properties for Utah FORGE 16A78-32 well. list the drilling fluid properties and formation geothermal properties.

Table 8: Drilling fluid properties for Utah FORGE 16A78-32 well.

	Unit	Value
Fluid density	ppg	9.0
Fluid plastic viscosity	lbf*s/100ft^2	27151
Specific heat capacity	BTU/(lb*°F)	0.907
Thermal conductivity	(BTU*in)/(hr*ft2*°F)	5.200

Table 9: Formation geothermal properties for Utah FORGE 16A78-32 well.

	Unit	Value
Formation surface temperature	°F	67.85
Formation temperature gradient	°F/ft	0.041
Rock density	ppg	23.367
Formation specific heat capacity	BTU/(lb*°F)	0.222
Formation thermal conductivity	(BTU*in)/(hr*ft2*°F)	16.016

3.2 Control Scenario: Using Both Mud Temperature at Inlet and Mud Pump Rate as Control Variables

This control scenario begins with the mud pump rate and mud temperature at inlet set to 400 gpm and 120 °F, respectively. By 200 minutes, the system reaches a steady state, and the controller is activated. The target pressure starts from its steady-state value prior to 200 minutes and increases by 80 psi over 10 minutes, while the target temperature decreases by 40 °F during the same period. The control variables and corresponding response variables are depicted in Figure 10. MIMO control response when mud pump rate and mud temperature at inlet are used.

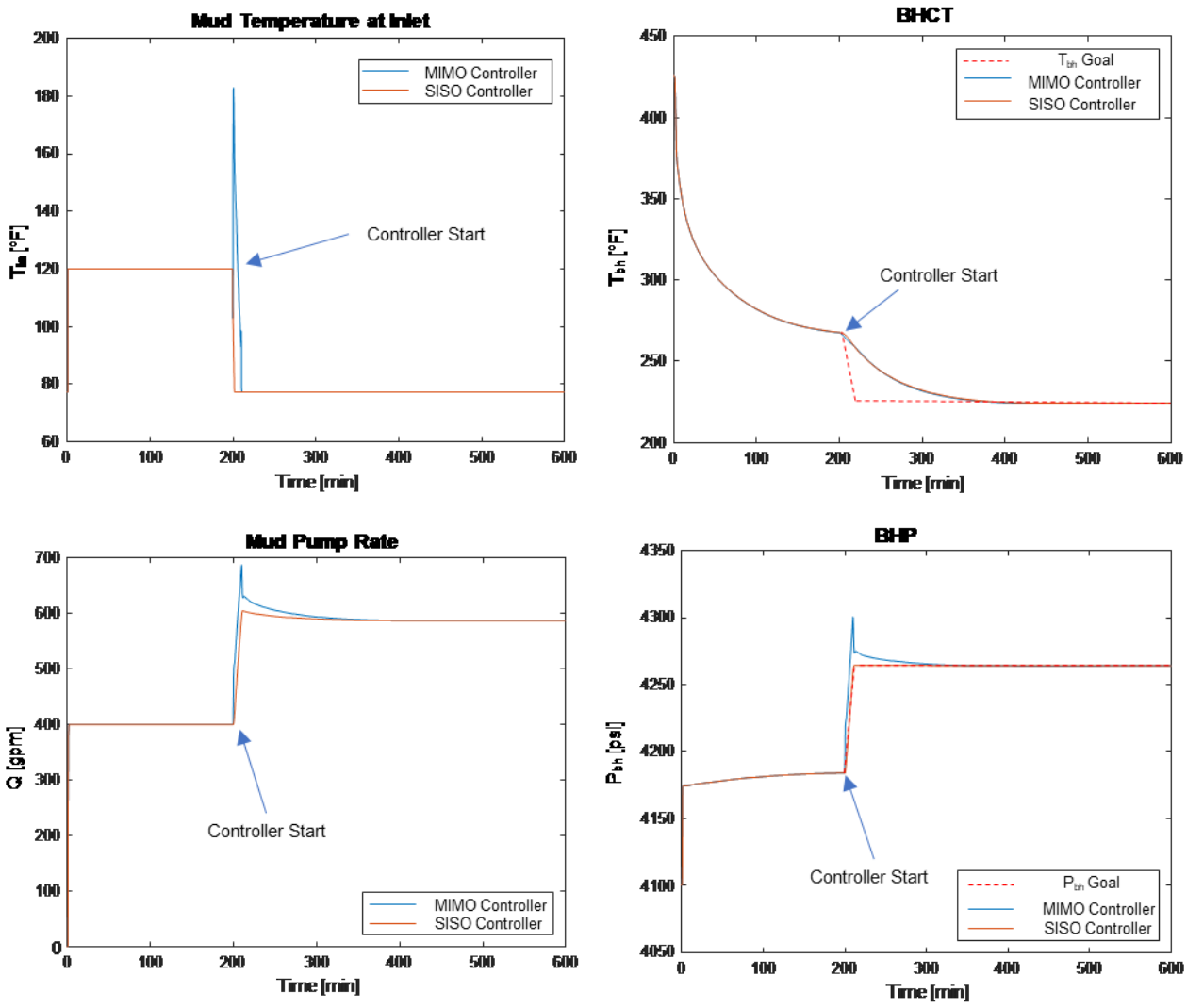

Figure 10. MIMO control response when mud pump rate and mud temperature at inlet are used.

It can be observed that the MIMO controller and the SISO controller perform similarly in regulating the BHCT. However, when controlling the BHP, the MIMO controller exhibits noticeable oscillations. These oscillations result from an overshoot in the mud pump rate, which is caused by the slow response of the BHCT. Furthermore, the MIMO controller demonstrates an undesirable spike in the mud temperature at inlet, occurring because the pressure responds so rapidly that it exceeds the target pressure.

In contrast, the SISO controller effectively regulates both the BHP and BHCT without oscillations or overshoot. This improved performance is attributed to the inherent differences in the natural frequencies of the two processes, which the SISO controller manages more effectively by eliminating cross-influences.

Thus, we conclude that in this scenario, the SISO controller outperforms the coupled controller by avoiding cross-coupling effects and delivering more stable control.

3.3 Control Scenario: Using Both Choke Opening and Mud Pump Rate as Control Variables

This control scenario begins with the mud pump rate and choke opening set to 400 gpm and 0.3, respectively. By 200 minutes, the system reaches a steady state, and the controller is activated. The target pressure starts from its steady-state value prior to 200 minutes and decreases by 30 psi over 10 minutes, while the target temperature decreases by 10 °F during the same period. The mud pump mud inlet temperature is set to be 77 °F during the whole process. The control variables and corresponding response variables are depicted in Figure 11. MIMO control response when mud pump rate and choke are used.

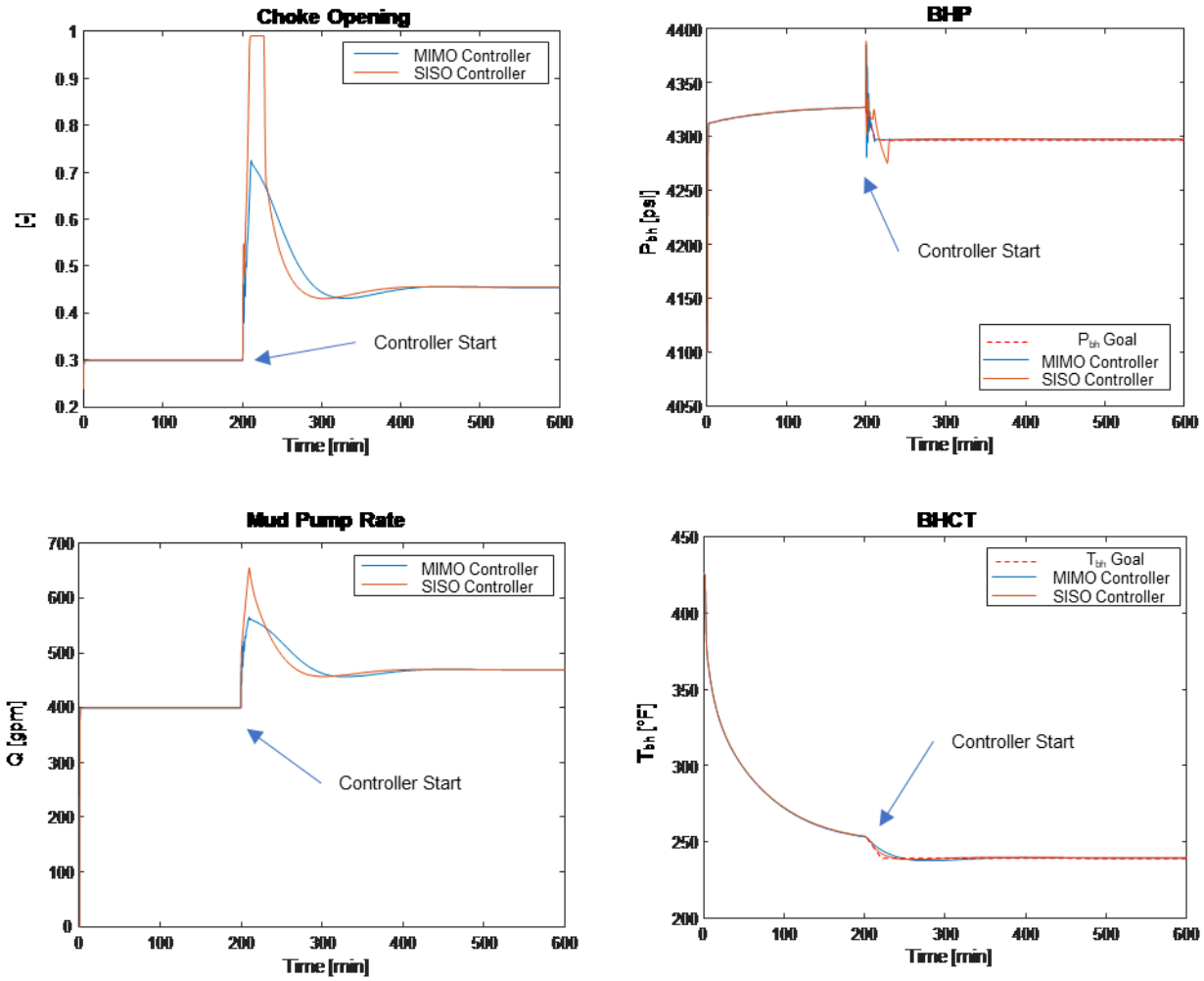

Figure 11. MIMO control response when mud pump rate and choke are used.

The MIMO controller achieves a slightly shorter settling time in regulating BHCT compared to the SISO controller. Additionally, it demonstrates superior performance in controlling BHP, with a shorter settling time and reduced overshoot. Moreover, the MIMO controller ensures smoother operation by minimizing variations in control variables, such as choke opening and mud pump rate. Therefore, the MIMO controller outperforms the SISO controller in this scenario, delivering more efficient and stable control.

4. CONCLUSION

This study introduces a novel coupled Managed Pressure and Temperature Drilling (MPD-MTD) control strategy using a MIMO control framework for combined and automate temperature and pressure management in geothermal and high-pressure, high-temperature (HPHT) wells. The proposed MPD-MTD approach leverages an improved reduced drift-flux model (RDFM) with enhanced pressure and temperature dynamics, offering excellent computational efficiency and accuracy for real-time control in extreme drilling environments.

Through simulations across various drilling scenarios, we compared the performance of MIMO and distributed SISO controllers using different control variable combinations. When employing mud pump rate and mud temperature at inlet as control variables, the distributed SISO controllers performed better, avoiding cross-coupling effects and ensuring greater stability. Conversely, with mud pump rate and choke opening as control variables, the coupled MIMO controller prevailed, achieving shorter settling times, reduced overshoot, and smoother operation by minimizing control variable fluctuations. These findings emphasize the need to tailor control strategies to specific operational objectives.

In conclusion, a coupled, automated MPD-MTD strategy is expected to surpass traditional methods to manage complex temperature and pressure situation and their interactions in the extreme well conditions of geothermal and HPHT wells. By integrating advanced modeling with robust MIMO control, the MPD-MTD approach enhances operational reliability, optimizes drilling performance, and mitigates thermal and pressure-related challenges sch as temperature-induced downhole tool failures. Future work will focus on field validation and extending applicability to more complex scenarios, including wells with variable mud properties, advanced cooling technologies, and dynamic drilling conditions.

ACKNOWLEDGEMENTS

We would like to thank the members of the Rig Automation and Performance Improvement in Drilling (RAPID) group at the University of Texas at Austin for their guidance and support.

REFERENCES

Aarsnes, U. J. F. (2016). Modeling of Two-Phase Flow for Estimation and Control of Drilling Operations [PhD thesis, Norwegian University of Science and Technology]. https://www.researchgate.net/publication/301834146

Ambrus, A., Vajargah, A. K., Ashok, P., & van Oort, E. (2017). Choke Controller Design for Automated MPD with Realistic Operational System Conditions. AADE. https://www.aade.org/application/files/1315/7132/1744/AADE-17-NTCE-095_-_Ambrus.pdf

Baer, M. R., & Nunziato, J. W. (1986). A two-phase mixture theory for the deflagration-to-detonation transition (ddt) in reactive granular materials. International Journal of Multiphase Flow, 12(6), 861–889. https://doi.org/10.1016/0301-9322(86)90033-9

Chatterjee, K., Aaron, D., & Macpherson, J. (2015). High Temperature 300°C Directional Drilling System. https://doi.org/10.2172/1208637

Fallah, A. H., Gu, Q., Chen, D., Ashok, P., & van Oort, E. (2021). Globally scalable geothermal energy production through managed pressure operation control of deep closed-loop well systems. Energy Conversion and Management, 236. https://doi.org/10.1016/j.enconman.2021.114056

Fallah, A. H., Gu, Q., Ma, Z., Karimi Vajargah, A., Chen, D., Ashok, P., van Oort, E., & May, R. (2020). Temperature dynamics and its effects on gas influx handling during managed pressure drilling operations. Journal of Natural Gas Science and Engineering, 83. https://doi.org/10.1016/j.jngse.2020.103614

Fjelde, K. K., Rommetveit, R., Merlo, A., & Lage, A. C. V. M. (2003, March 25). Improvements in Dynamic Modeling of Underbalanced Drilling. IADC/SPE Underbalanced Technology Conference and Exhibition. https://doi.org/10.2118/81636-MS

Garnier, H., Mensler, M., & Richard, A. (2003). Continuous-time model identification from sampled data: Implementation issues and performance evaluation. International Journal of Control, 76(13), 1337–1357. https://doi.org/10.1080/0020717031000149636

Gu, Q., Fallah, A., Ambrus, A., Chen, D., Ashok, P., & van Oort, E. (2019, March 22). Higher Precision Automated Managed Pressure Drilling Control Achieved Through the Addition of a Thermal Model. Day 3 Thu, March 28, 2019. https://doi.org/10.2523/IPTC-19326-MS

Gu, Q., Fallah, A. H., Ambrus, A., Feng, T., Chen, D., Ashok, P., & van Oort, E. (2022). Computationally efficient simulation of non-isothermal two-phase flow during well construction using a new reduced drift-flux model. Applied Thermal Engineering, 206. https://doi.org/10.1016/j.applthermaleng.2022.118077

Khaled, M. S., Wang, N., Ashok, P., & van Oort, E. (2023). Downhole heat management for drilling shallow and ultra-deep high enthalpy geothermal wells. Geothermics, 107. https://doi.org/10.1016/j.geothermics.2022.102604

Ljung, L. (2009). Experiments with Identification of Continuous Time Models. https://doi.org/10.3182/20090706-3-FR-2004.0209

Luu, A., Wang, N., Gu, Q., Khaled, M., Ashok, P., Chen, D., & Van Oort, E. (2024). Managed Temperature Drilling: An Automated Real-Time Controller for Downhole Temperature Control in Geothermal and HPHT Wells. SPE - International Association of Drilling Contractors Drilling Conference Proceedings, 2024-March. https://doi.org/10.2118/217747-MS

Ma, Z., Vajargah, A. K., Ambrus, A., Ashok, P., Chen, D., van Oort, E., May, R., Macpherson, J. D., Becker, G., & Curry, D. A. (2016). Multi-Phase Well Control Analysis During Managed Pressure Drilling Operations. SPE Annual Technical Conference and Exhibition, 26–28. https://doi.org/10.2118/181672-MS

Udegbunam, J. E., Fjelde, K. K., Evje, S., & Nygaard, G. (2014, April 8). A Simple Transient Flow Model for MPD and UBD Applications. SPE/IADC Managed Pressure Drilling & Underbalanced Operations Conference & Exhibition. https://doi.org/10.2118/168960-MS

Utah Forge Data. (2022). https://gdr.openei.org/forge (accessed May 2022).

van Oort, E., Chen, D., Ashok, P., & Fallah, A. (2021, March 8). Constructing Deep Closed-Loop Geothermal Wells for Globally Scalable Energy Production by Leveraging Oil and Gas ERD and HPHT Well Construction Expertise. SPE/IADC International Drilling Conference and Exhibition. https://doi.org/10.2118/204097-MS

Xu, Z., Song, X., Li, G., Zhu, Z., & Zhu, B. (2019). Gas kick simulation in oil-based drilling fluids with the gas solubility effect during high-temperature and high-pressure well drilling. Applied Thermal Engineering, 149, 1080–1097. https://doi.org/10.1016/j.applthermaleng.2018.12.110

Yang, H., Li, J., Liu, G., Jiang, H., Wang, C., & Jiang, J. (2019). A transient hydro-thermo-bubble model for gas kick simulation in deep water drilling based on oil-based mud. Applied Thermal Engineering, 158, 113776. https://doi.org/10.1016/j.applthermaleng.2019.113776